Geophysical Research Letters

Supporting Information for

Fate of warm Pacific water in the Arctic basin

Peigen Lin[1]*, Robert S. Pickart[1], Kjetil Våge[2], Jianqiang Li[3]

1. Woods Hole Oceanographic Institution, Woods Hole, MA, USA

2. Geophysical Institute, University of Bergen and Bjerknes Centre for Climate Research, Bergen, Norway

3. State Key Laboratory of Marine Environmental Science, College of Ocean and Earth Sciences, Xiamen University, Xiamen, China

*Corresponding author. Email: plinwhoi@gmail.com

Contents of this file

Introduction

We describe the details of the historical velocity dataset in Text S1, and show the data coverage of the historical hydrography and velocity in space and time in Figure S1. In Text S2, we demonstrate that the along-canyon wind from the meteorological station in Utqiaġvik is significantly correlated with that from the ERA5 reanalysis over a broad region of Barrow Canyon. In Text S3 and Figure S2 we present the rationale for carrying out the water mass end-member analysis in potential density/potential spicity (σ/π) space. Text S4 describes the results of an empirical orthogonal function analysis demonstrating that the dominant flow variability in Barrow Canyon is controlled by the local along-canyon wind. Text S5 provides the methods of gridding and determining the lag time of velocity and hydrography with respect to the wind forcing. Supplementary to the main text (Fig. 2), Text S6 and Figure S3 show the velocity and hydrographic responses to the cross-canyon wind in Regime 3.

Text S1.

The velocity dataset used in this study (Fig. S1c, d) was constructed using shipboard acoustic Doppler current profiler (ADCP) data from 47 cruises from 2002 to 2018, including 33 USCGC *Healy* cruises, 7 R/V *Sikuliaq* cruises, and 7 R/V *Mirai* cruises. The data were collected using the University of Hawaii UHDAS software, except for the early cruises in 2002-04 collected with VMDAS. Standard quality control procedures were applied to the dataset, including bottom- and water-track calibrations, single-ping and ensemble-ping editing, and ship's heading checks. A subset of these cruises had previously received additional post-cruise processing as part of other research projects. The remainder was visually edited for standard issues such as bottom or ice interference. Previously applied calibrations and heading corrections via secondary heading feeds were checked and, in a few cases, mildly adjusted.

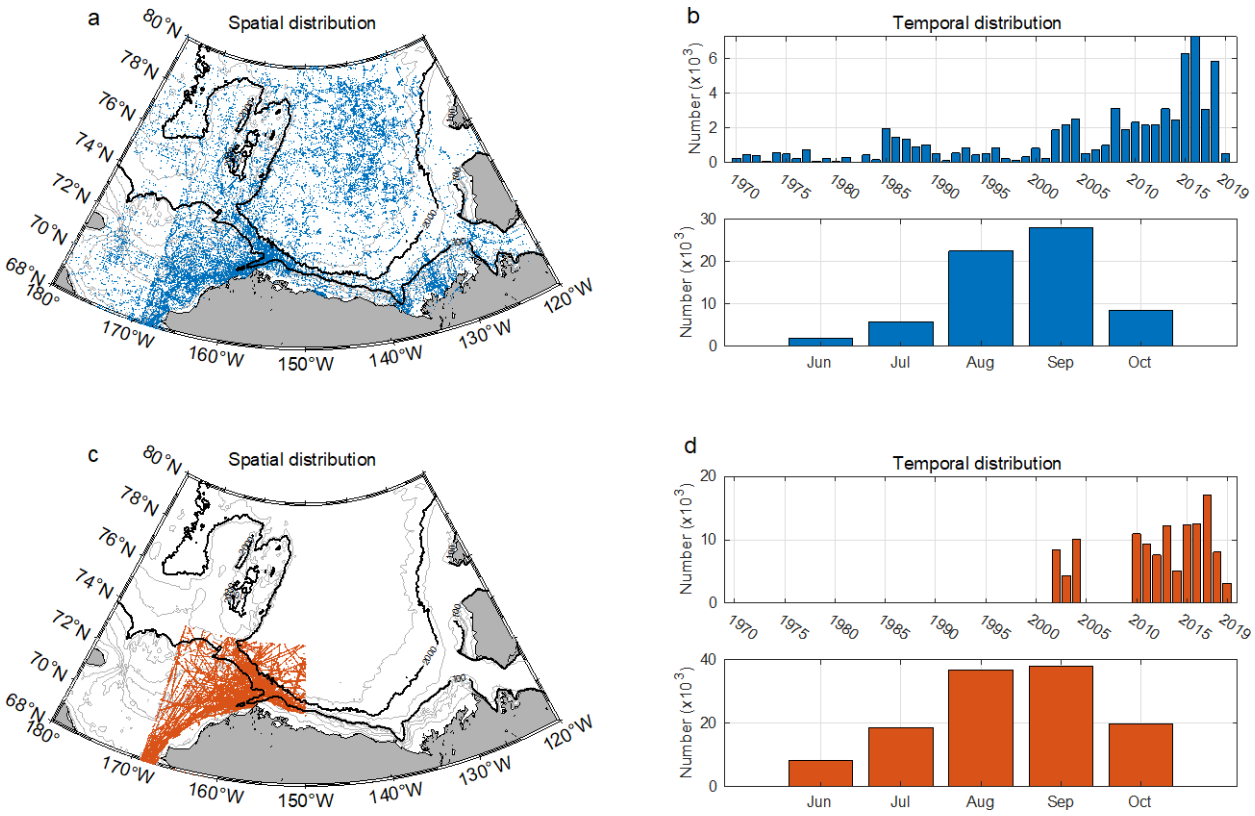

Figure S1. Data coverage of the composite historical hydrography and velocity datasets in space and time. (a, b) historical hydrographic profiles, and (c, d) historical shipboard ADCP velocity data.

Text S2.

Within the domain of Fig. 2 we computed the correlation between the along-canyon wind from the Utqiaġvik weather station and the ERA5 reanalysis wind (ERA5 is a reanalysis product from the European Center for Medium-Range Weather Forecasts, Hersbach (2018)) over the period 1979-2020. The mean correlation coefficient is 0.85 ($p<0.01$), with a maximum value of 0.95. This suggests that the wind data from the Utqiaġvik weather station are representative of the vicinity of Barrow Canyon as a whole. It is consistent with many previous studies in this region which have widely used the weather station wind (Lin, Pickart, McRaven, et al., 2019; Pickart et al., 2019; Pisareva et al., 2019).

Text S3.

Previous studies have analyzed water mass distributions in the Chukchi and Beaufort Seas using defined potential temperature/salinity (θ/S) boundaries (Lin et al., 2016; Pickart et al., 2019; Pisareva et al., 2019), or using an end-member approach (Lin, Pickart, McRaven, et al., 2019). Using the historical hydrographic data over the domain shown in Fig. S1a, we constructed a volumetric θ/S diagram over the depth range 0-100 m (we do not consider the Atlantic Water at depth) (Fig. S2a). On the diagram we have marked what could be considered end-members of PSW, PWW, MWR-cold, and MWR-warm. Unfortunately, it is extremely difficult to classify a given parcel of water in terms of four end-members; typically this is done using three end-members. This motivated us to use potential density/potential spicity (σ/π) space (Fig. S2b), which has been used effectively for water mass classification and analysis in the Nordic Seas (Huang et al., 2020) and in the South China Sea (Gao et al., 2020).

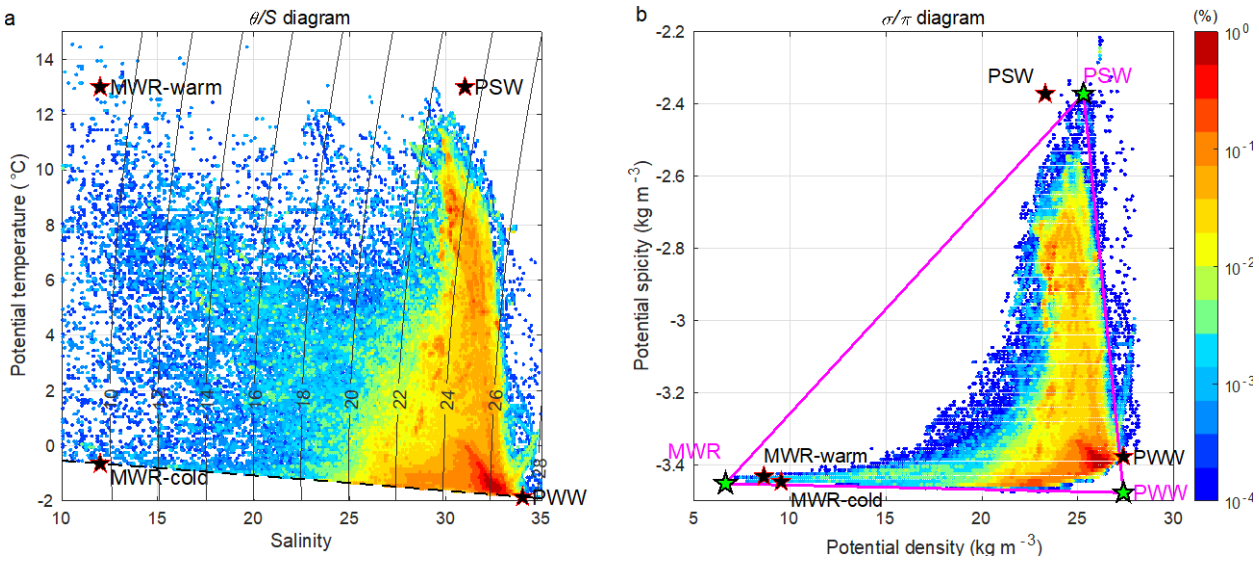

Figure S2. Definitions of water mass end-members. (a) Volumetric potential temperature/salinity (θ/S) diagram using the historical hydrographic data in the upper 100 m. The three main water masses are Pacific Summer Water (PSW), Pacific Winter Water (PWW), and two components of sea-ice meltwater / river runoff water (MWR-cold and MWR-warm). The black dashed line is the freezing point temperature. (b) Same as (a) except in the potential density/potential spicity (σ/π) plane. The black stars and font denote the water mass end-members in (a). The magenta lines

denote the mixing triangle associated with the three σ/π end-members (green stars): PSW, PWW and MWR.

Text S4.

We quantified the contribution of the local along-canyon wind to the outflow through Barrow Canyon as follows. Using the year-long ADCP data from a mooring situated near the head of the Barrow Canyon in 2012-2013 (the BC2 mooring in Weingartner et al. (2017)), we applied an empirical orthogonal function (EOF) analysis to the timeseries of the velocity profile. The dominant EOF mode (EOF1) accounts for 79% of the variance. The principal component timeseries for EOF1 is significantly correlated with the local along-canyon wind speed ($R=0.61$, $P<0.01$). We also did the same exercise for the velocity data (upper 100 m) from a mooring at the mouth of the canyon in 2012-2013 (Itoh et al., 2015). This returned a similar result: EOF1 explains 90% of the variance, correlated with the along-canyon wind ($R=0.65$, $P<0.01$). These results indicate that the variation of the flow in Barrow canyon is significantly controlled by the local wind.

Text S5.

While the historical hydrographic data have been previously quality controlled, additional error checking was nonetheless applied following previous methodology (Våge et al., 2013). Profiles containing a density inversion greater than 0.05 kg m^{-3} were identified, and the data points in question removed. To map the data in geographical space, we use an interpolation scheme where the search radius has enhanced weighting along the isobaths (Davis, 1998) instead of an isotropic weighting in all directions. The spatial resolution of the gridding varied depending on the size of the domain in question, ranging from 0.2°×0.1° (longitude, latitude) for the vicinity of Barrow Canyon to 1°×0.5° for the full domain. The composite vertical section across the Chukchi slope and Northwind Ridge was constructed using all profiles within a distance of 25 km from the line, and was gridded using Laplacian-Spline interpolation (Smith & Wessel, 1990) with a grid spacing of 20 km in the horizontal and 2 m in the vertical. For the along-isobath section, a coarser

resolution of 50 km × 5 m was used to include more data for each grid point. The gridded data were further smoothed using a 3×3 window.

For the analysis of the Barrow Canyon region, we accounted for the delay time between the wind forcing and velocity and density response by using the mooring data at the mouth of the Barrow Canyon from 2012-13 (Itoh et al., 2015), published by Japan Agency for Marine-Earth Science and Technology (JAMSTEC). We considered the along-canyon component of flow (56°T) (Pisareva et al., 2019), and computed the lag correlation between the timeseries of velocity averaged over the upper 100 m and the along-canyon wind (52°T) from the Utqiaġvik wind product. This indicated that the velocity response lagged the wind by 6 hrs. The same calculation for the average density in the upper 100 m gives a lag of 15 hrs. These delay times are comparable to previous upwelling studies in Barrow Canyon and on the Alaskan Beaufort slope (Pisareva et al., 2019; Schulze & Pickart, 2012). While the lag time can change slightly with different wind speeds, our results were not sensitive to this. A similar lag for velocity and density was computed for the Beaufort slope using previously collected mooring data from 152°W (Lin, Pickart, Moore, et al., 2019).

Text S6.

For the case when the along-canyon wind speed in Barrow Canyon is negligible (-2 to 2 m s^{-1}), the winds are mainly in the cross-canyon direction (along the slope); i.e., southeasterly and northwesterly. We thus suspect that the cross-canyon wind predominantly dictates the velocity structure and the PSW distribution. To demonstrate this, we applied the same technique for constructing composite velocity and PSW percentage maps for each of the two cross-canyon wind conditions (Fig. S3). For southeasterly wind, the westward-flowing slope current is intensified, particularly in vicinity of the canyon mouth, which facilitates the transfer of PSW to the west. In contrast, when the wind is northwesterly, the velocity vectors on the Chukchi slope become disorganized while the Beaufort Shelfbreak Jet is well established. Accordingly, the PSW is mainly found east of Barrow Canyon.

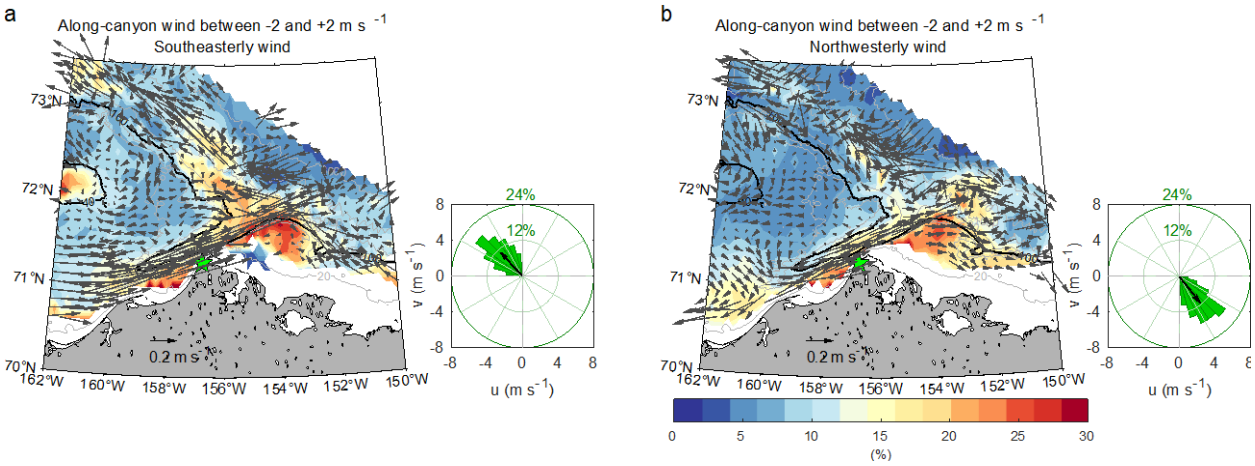

Figure S3. Composite velocity and PSW percentage maps for the two cross-canyon wind regimes. (a) Southeasterly wind and (b) northwesterly wind, when the along-canyon wind speed is from -2 to 2 m s^{-1} (Fig. 2). The vectors are the vertically-averaged velocity in the upper 100 m and the colors denote the PSW percentage at 30 m. The 40 m and 100 m isobaths are highlighted by thick lines. The wind rose and mean wind vector for each scenario are computed using the data from Utqiaġvik weather station (green star on the map).